

Article

Ammonium and Tetraalkylammonium Salts as Additives for Li Metal Electrodes

Dario Di Cillo, Luca Bargnesi, Giampaolo Lacarbonara and Catia Arbizzani * 

Department of Chemistry “Giacomo Ciamician”, Alma Mater Studiorum–University of Bologna, 40126 Bologna, Italy

* Correspondence: catia.arbizzani@unibo.it

Abstract: Lithium metal batteries are considered a promising technology to implement high energy density rechargeable systems beyond lithium-ion batteries. However, the development of dendritic morphology is the basis of safety and performance issues and represents the main limiting factor for using lithium anodes in commercial rechargeable batteries. In this study, the electrochemical behaviour of Li metal has been investigated in organic carbonate-based electrolytes by electrochemical impedance spectroscopy measurements and deposition/stripping galvanostatic cycling. Low amounts of tetraalkylammonium hexafluorophosphate salts have been added to the electrolytes with the aim of regulating the lithium deposition/stripping process through the electrostatic shielding effect that improves the lithium deposition. The use of NH_4PF_6 also determined good lithium deposition/stripping performance due to the chemical modification of the native solid electrolyte interphase via direct reaction with lithium.

Keywords: lithium metal interphase; ammonium salts; protonated salt; impedance spectroscopy

1. Introduction

Li-ion batteries (LIBs) are the most successful batteries on the market, suitable for a wide range of applications due to their high specific energy and power. Their success came from the safety issues that scientists faced when using a Li metal anode in rechargeable cells [1,2]. The substitution of graphite as anode has created modern LIBs. However, performance requirements have changed over the last several decades, and the demand for more specific energy and power has been increasing, specifically in the automotive field. Li metal anodes seem to again be cutting edge, and have been proposed for the most advanced batteries, namely Gen 4 and Gen 5 configurations [3]. The reactivity of the electrolyte, both with Li metal and graphite anodes, is the main reaction responsible for cell cycling stability. The reaction produces a layer on the anode, i.e., the solid electrolyte interphase (SEI), that prevents further reactions of the electrolyte. Understanding the phenomena governing SEI formation and its dynamics is crucial, especially in the research field of Gen 4 and Gen 5 batteries. Li reacts almost instantly with most organic solvents, forming an SEI layer whose chemical composition and characteristics are strictly dependent on the nature of the solvent and the dissolved salts. In the case of alkyl carbonate electrolytes, the major constituents of the SEI are alkyl lithium carbonates (ROCO_2Li), formed by one-electron reduction followed by a radical termination reaction. Radical reaction pathways can easily lead to various products, and species with Li–C bonds can be formed [4–6]. An SEI with good mechanical stability, good adhesion to the underlying metal surface, and a chemical composition ensuring low solubility in the electrolyte is required. A SEI layer made of elastic and flexible components could accommodate the volume change and stabilize the interphase during cycling. The stable passivation of the surface by a layer with infinitesimally small electronic conductivity is crucial to prevent further consumption of the electrolyte and the active material itself, which is the main cause of reduced coulombic efficiency and



Citation: Di Cillo, D.; Bargnesi, L.; Lacarbonara, G.; Arbizzani, C. Ammonium and Tetraalkylammonium Salts as Additives for Li Metal Electrodes. *Batteries* **2023**, *9*, 142. <https://doi.org/10.3390/batteries9020142>

Received: 29 December 2022

Revised: 9 February 2023

Accepted: 14 February 2023

Published: 20 February 2023



Copyright: © 2023 by the authors. Licensee MDPI, Basel, Switzerland. This article is an open access article distributed under the terms and conditions of the Creative Commons Attribution (CC BY) license (<https://creativecommons.org/licenses/by/4.0/>).

capacity fading. Eventually, high Li^+ conductivity is needed to prevent overpotentials due to concentration polarization of the cell upon charge/discharge cycles [7].

Tetraalkylammonium cations are often components of ionic liquids with a wide electrochemical window. However, these electrochemically stable electrolytes are highly viscous compared to organic electrolytes, which sometimes results in poor electrochemical performance [8]. When tetraalkylammonium salts are used as additives in organic electrolytes, the viscosity remains relatively low and the stability window wide. In addition, hexafluorophosphate anion has been demonstrated to be beneficial even at low concentrations [9], so that in absence of lithium hexafluorophosphate as the main salt, the advantage of hexafluorophosphate anion as an additive can be exploited.

Another critical aspect deals with Li dendrite growth. During plating, a cation concentration gradient is formed between the electrodes. When the current density is above a critical value, it can only be sustained for a definite period, called Sand's time, after which the cations near the plated electrode surface run out. Cation depletion causes the rupture of electrical neutrality, building up a local space charge, which gives rise to the formation of branched metal deposits [10]. The presence of the SEI layer induces localized variations in the molar volume of the electrodeposited material [11]. In general, protrusions possess a considerably higher electric field at their tips and tend to attract more lithium ions with respect to flat parts. For very low current densities ($\sim 0.1 \text{ mA cm}^{-2}$) a relatively planar morphology is favored. Due to fast mass accretion, the system becomes diffusion-limited for very high current densities ($\sim 10 \text{ mA cm}^{-2}$), inducing large concentration depletion gradients in front of the dendrite so that a highly branched morphology is formed [12].

Blocking lithium dendrite growth is the main path toward developing safer batteries with prolonged cycle life. The most intuitive approach is to provide a physical barrier to the accretion of dendrites, using a separator with high elastic modulus, so that the tips of lithium dendrites are bent and, thus, unable to pass through the separator [13,14]. Alternatively, the electrolyte composition can be tailored to stabilize the metal–electrolyte interphase limiting the lithium dendritic electrodeposition [15].

For this purpose, solvents and salts can be varied to modify the composition of SEI. Ethylene carbonate exhibits a peculiar film-forming ability by reduction at 0.8 V vs. Li. It is used as a cosolvent in mixtures with other carbonates to form a good SEI, thus preventing continuous electrolyte consumption. However, this is still insufficient to inhibit the formation of dangerous cracks and dendrites in Li metal anodes. Several additives have also been proposed to improve SEI quality, such as vinylene carbonate [16], fluoroethylene carbonate [17], and ethylene sulfides [18,19], that produce a very stable layer in carbonate-based electrolytes. SEI-forming sacrificial additives are extensively used to enrich the SEI layer of inorganic and organic species, such as LiF , Li_2CO_3 , Li_xNO_y , Li_3N , or species derived from polymerization reactions [20,21]. In ether-based electrolytes, LiNO_3 or additives that produce a Li_3N layer on Li metal are favorable to form a stable SEI in lithium/sulfur batteries [22,23].

A viable strategy to limit the dendritic growth is facilitating the mass transport of lithium ions in the electrolyte. For this purpose, new types of additives, such as zwitterionic compounds, are used to promote ion dissociation and improve the ion conductivity of the electrolytes [24]. Alternatively, additives with electron-deficient properties, such as substituted boranes and phosphines, can sequester the anions from the Li^+ solvation shell, increasing its mobility [25]. Another approach was suggested by Ding et al. who prevented the formation of dendritic Li by a self-healing electrostatic shield mechanism, introducing Cs^+ cations. These cations form a positively charged electrostatic shield on the lithium protuberances during the Li deposition, thus mitigating the formation of Li dendrites [26].

This work aims to study the lithium metal–electrolyte interphase, which is crucial in determining the lithium electrode behavior. The electrochemical properties of two carbonate-based electrolytes with the addition of ammonium and tetraalkylammonium salts have been explored. To our knowledge, this is the first time that ammonium salts have

been investigated as additives for Li batteries. Electrochemical impedance spectroscopy, cyclic voltammetry and galvanostatic charge, and discharge measurements were used to evaluate the effect of additives on the SEI layer and on the electrochemical performance. Ammonium hexafluorophosphate (NH_4PF_6) has been investigated to perform an in situ chemical modification of the native SEI layer. In contrast, tetramethylammonium hexafluorophosphate (TMAPF_6) and tetraethylammonium hexafluorophosphate (TEAPF_6) have been used with the idea of limiting the formation of dendrites by electrochemically stable additives that electrostatically cover the lithium asperities inducing a smoother plating.

2. Materials and Methods

2.1. Electrode and Electrolytes Preparation

For electrode and electrolyte preparation, we used the following chemicals: lithium metal ribbon (Sigma Aldrich, 0.75 mm thick, 99.9%, Merck KGaA, Darmstadt, Germany), $\text{LiNi}_{1/3}\text{Mn}_{1/3}\text{Co}_{1/3}\text{O}_2$ (NMC) electrode, 1 M LiPF_6 in ethylene carbonate:dimethylcarbonate (EC:DMC) 1:1 wt/wt (LP30, Solvionic, 99.9%, Solvionic, Toulouse, France), propylene carbonate (PC, Sigma Aldrich, >99%, Merck KGaA, Darmstadt, Germany), lithium bis(trifluoromethanesulfonyl)imide (LiTFSI , Sigma Aldrich, 99.5%, Merck KGaA, Darmstadt, Germany), ammonium hexafluorophosphate (NH_4PF_6 , Fluorochem Co., >99%, Fluorochem Limited, Glossop, UK), tetramethylammonium hexafluorophosphate (TMAPF_6 , Sigma Aldrich, >99%, Merck KGaA, Darmstadt, Germany), tetraethylammonium hexafluorophosphate (TEAPF_6 , Sigma Aldrich, >99%, Merck KGaA, Darmstadt, Germany). The electrolyte solutions were 1 M LiPF_6 in EC:DMC 1:1 wt/wt (LP30), and 1 M LiTFSI in PC. These solutions are indicated in the following as LP30, and PC, respectively. The ammonium and alkyl ammonium salt additives were 50 mM, which is about 1 wt.%. Solutions with the additives are indicated with the name of the solution and the name or abbreviations of the additive, i.e., NH_4PF_6 , TMAPF_6 , TEAPF_6 .

2.2. Cell Assembly

Two- and three-electrode electrochemical cells have been assembled in a glovebox (Mbraun Labmaster SP, MBraun Inc., Stratham, NH, USA) in an inert argon atmosphere ($\text{O}_2 < 0.1$ ppm and $\text{H}_2\text{O} < 0.1$ ppm). A conventional cell (Lithium Battery Cell Gamry, Gamry Instruments, Warminster, PA, USA) with stainless steel working and counter electrodes (0.38 cm^2), and a Li reference electrode was used to evaluate the electrochemical stability window of the electrolytes by cyclic voltammetry. The deposition/stripping process of Li by cyclic voltammetry was evaluated in Teflon T-shaped cells (BOLA, Bohlender GmbH, Grünsfeld, Germany) (0.785 cm^2), with the bare stainless steel plunger used as the working electrode and the Li foil as the counter electrode (two-electrode mode). Stainless steel T-shaped cells (Swagelok, Swagelok Company, Cleveland, OH, USA) with stainless steel plungers were used for the galvanostatic Li deposition/stripping processes and electrochemical impedance spectroscopy (EIS), in two-electrode mode with a Li foil on both plungers (0.88 cm^2). BOLA and Swagelok cells have been assembled with glass microfiber separators (Whatman, GF/A) predried in an oven (B-585 Kugelrohr, BÜCHI Labortechnik AG, Flawil, Switzerland) at $120 \text{ }^\circ\text{C}$ under vacuum for 12 h.

2.3. Physicochemical and Electrochemical Characterization

The electrochemical tests, including EIS, have been performed with a BioLogic VSP potentiostat/galvanostat (Biologic, Seyssinet-Pariset, France). The galvanostatic cycling with potential limitation (GCPL) measurements of $\text{Li}||\text{Li}$ cells were carried out at three values of the current density to evaluate the deposition/stripping of lithium under different conditions. The impedance spectra were carried out in the $100 \text{ kHz}-0.1 \text{ Hz}$ frequency range, at $\pm 10 \text{ mV}$ alternating voltage and collecting 10 points per decade. The test protocol was the following: EIS (t_0); 10 GCPL cycles at 0.125 mA cm^{-2} ; EIS (t_1); 10 GCPL cycles at 0.250 mA cm^{-2} ; 100 GCPL cycles at 0.500 mA cm^{-2} ; 10 GCPL cycles at 0.125 mA cm^{-2} ; EIS (t_2); prolonged GCPL cycling at 0.125 mA cm^{-2} . Each GCPL cycle lasts for 1 h (30 min

oxidation and 30 min reduction). To simplify the discussion, the EIS measurements will be indicated following their order in time as t_0 , t_1 , and t_2 . All the electrochemical tests were carried out on the cell placed in a thermostatic oven at 30 °C. X-ray diffractograms (XRD) were collected on carbon powders by using an x-ray diffractometer PANalytical X'Pert PRO (Malvern Panalytical, Malvern, UK) equipped with an X'Celerator detector (Cu $K\alpha$ radiation, 40 mA, 40 kV).

Scanning electron microscopy (SEM) images were acquired with SEM Leica/Cambridge Stereoscan 360 and software package INCA. Lithium electrodes were cycled in the electrolytes under investigation following the reported test protocol: 10 GCPL cycles at 0.125 mA cm⁻²; 5 GCPL cycles at 0.250 mA cm⁻²; 5 GCPL cycles at 0.500 mA cm⁻²; 10 GCPL cycles at 0.125 mA cm⁻². The cells were disassembled in a glovebox, and the Li electrodes, which were placed on SEM stabs, were sealed in vials to minimize air exposure before transferring them onto the SEM holders.

3. Results

3.1. Electrochemical Investigations

Cyclic voltammetry has been used to explore the electrochemical stability window of the electrolytes. Figure 1 displays the cyclic voltammograms (CVs) at 20 mV s⁻¹ between 0.050–5 V for the LP30 and PC, without and with additives. LP30 is the most stable solution. The presence of the additives enhances the reduction current. The reduction process starts around 1.5 V in each system, and the reduction current can be reasonably attributed to the electrolyte decomposition, which is strongly affected by the presence of NH₄PF₆. The current density values are notably increased by NH₄PF₆ and its behavior appears clearly different from that of the alkyl ammonium salts. In oxidation, both LP30 and PC are sufficiently stable up to 5 V, making their use compatible with high voltage operating cathodes such as NMC and LiNi_{0.5}Mn_{1.5}O₄. The oxidation peaks between 1.5 and 2.0 V in the reverse scan are present in all the plots, although they are less visible in the LP30-based set. This is probably due to some impurity or a specific process involving the stainless steel electrode surface.

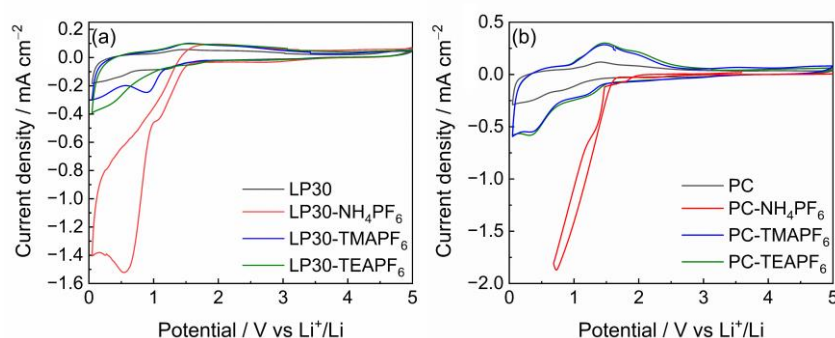


Figure 1. CVs at 20 mV s⁻¹ of (a) LP30 and (b) PC without and with the addition of 50 mM of NH₄PF₆, TMAPF₆, and TEAPF₆.

The lithium deposition/stripping process has been studied in a two-electrode set up on stainless steel working electrode. The CVs are reported in Figure 2. In all the electrolytes, NH₄PF₆ seems to facilitate the deposition, causing a shift in the onset reduction (onset reduction and oxidation peak values from the first CV cycle are reported in Table A1 in Appendix A), anticipating the beginning of the process, which starts at higher potential values. Both TMAPF₆ and TEAPF₆ show similar reduction onsets that make the deposition in propylene carbonate electrolyte slightly easier during the first cycles. This effect, however, is gradually lost. The oxidation peak potentials are variously shifted depending on the cycle so that a clear trend about the effect of the additives cannot be rationalized. The same is true for the variation in the current density with cycling. When ammonium ion is present,

the current is higher but tends to decrease with cycling. This is particularly evident for LP30-NH₄PF₆ but is less pronounced for PC-NH₄PF₆.

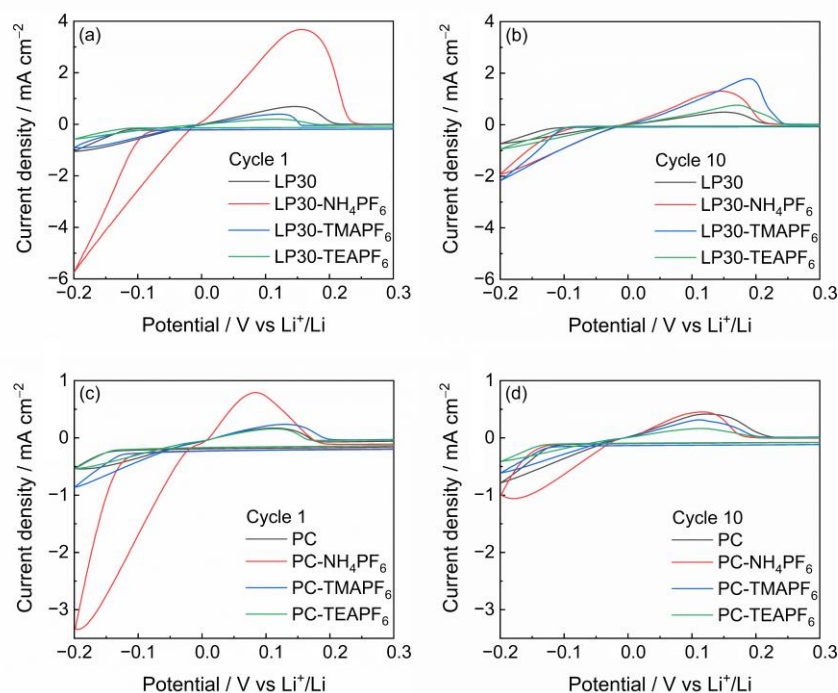


Figure 2. CVs at 20 mV s⁻¹ of (a) 1st CV, (b) 10th CV in LP30, and (c) 1st CV, (d) 10th CV in PC without and with the addition of 50 mM of NH₄PF₆, TMAPF₆ and TEAPF₆.

LP30 with the two alkylammonium additives show similar behavior, which results in increasing current with cycling and in shifting the oxidation peak towards higher potentials. The CVs of PC with the two alkylammonium additives do not seem to vary with the number of cycles.

The GCPL cycles of the Li || Li symmetric cells in LP30 are reported in Figure 3a. The cell shows a constantly diminishing overvoltage during the final prolonged cycling at the lowest current density, which is likely related to the increased electrode surface area generated by dendritic electrodeposition. LP30-NH₄PF₆ in Figure 3b displays even lower overvoltage than LP30 at 0.125 and 0.250 mA cm⁻². During and after cycling at 0.500 mA cm⁻², the overvoltage profile is considerably increased. The overvoltage, with a slightly increasing trend, reaches a maximum value of about 55 mV when the current density was brought again to the lowest value. LP30-TMAPF₆ (Figure 3c) behaves similarly to LP30 but shows a less regular profile with some abrupt change in the overvoltage (see at 900 h). This is compatible with the detachment of dendrites, which could have caused a sudden decrease in the electrode surface. LP30-TEAPF₆ (Figure 3d) shows similar behavior to LP30-TMAPF₆, but it has a higher overpotential at 0.500 mA cm⁻² and a staircase profile around 150 h of functioning. The latter could be explained by a massive dendritic accretion. The low values of overvoltage after prolonged cycling could also be due to the reduced effectiveness of the glass fiber separator, whose mechanical integrity can be damaged by the formation of small amounts of HF generated by the reaction between LiPF₆ and traces of water.

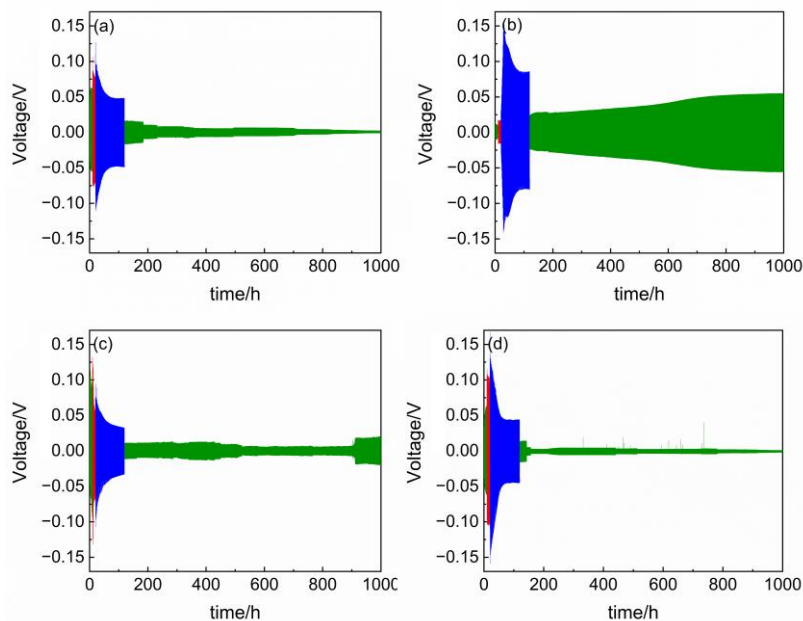


Figure 3. Deposition and stripping cycles of Li | Li symmetric cells with (a) LP30, (b) LP30-NH₄PF₆, (c) LP30-TMAPF₆, (d) LP30-TEAPF₆ electrolytes at 0.125 mA cm⁻² (green), 0.250 mA cm⁻² (red) and 0.500 mA cm⁻² (blue).

Compared with LP30-based solutions, the symmetric cells in PC-based solutions, as reported in Figure 4a–d, showed a higher overvoltage, which is appropriate for the electrolyte system. PC (Figure 4a) reaches 300 mV overvoltage during the first cycles at the higher current. Coming back to the lowest current value, the cell reaches the same overvoltage of the starting cycles. In the long run, the stability of the overvoltage profile is affected by a constant rise resulting from the formation of a thick layer of dead lithium observed after the cell disassembly.

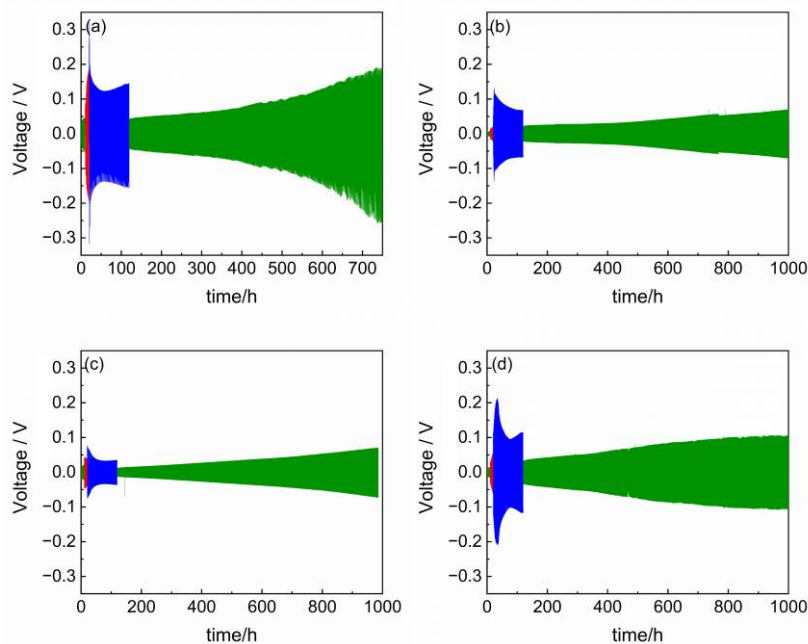


Figure 4. Deposition and stripping cycles of Li | Li symmetric cells with (a) PC, (b) PC-NH₄PF₆, (c) PC-TMAPF₆, (d) PC-TEAPF₆ electrolytes at 0.125 mA cm⁻² (green), 0.250 mA cm⁻² (red) and 0.500 mA cm⁻² (blue).

The cell with the PC electrolyte is likely to be affected by the concomitant effect of dead lithium accumulation and electrolyte depletion in the last 500 h. Both effects worsen the performance of the cell, which exhibits a strong asymmetric polarization profile. All the investigated additives, i.e., NH_4PF_6 , TMAPF_6 , and TEAPF_6 , appear to both be helpful in decreasing the overpotential and have a stabilization effect (Figure 4b,d).

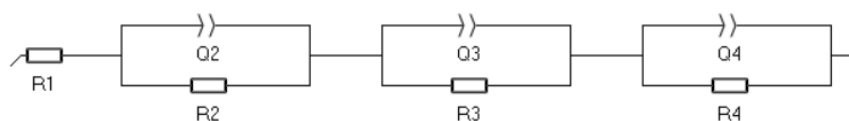
3.2. Impedance Spectroscopy Investigation

The impedance spectra were fitted using equivalent circuits composed by resistors and constant phase elements, respectively indicated as R and Q. The constant phase elements replace the ideal capacitors in the equivalent circuit when the system displays the nonideal capacitive behaviour that originates from the rough and imperfect surface with the characteristic depressed shape of the semicircles or sloped lines [27]. The impedance of the constant phase element is

$$Z_{\text{CPE}} = 1/[Q(i\omega)^a] \quad (1)$$

with $\omega = 2\pi\nu$ and having Q the dimension F s^{a-1} (or $\Omega^{-1} \text{s}^a$).

Different equivalent circuits have been used depending on the spectrum. For the equivalent circuit $R_1(R_2/Q_2)(R_3/Q_3)(R_4/Q_4)$ (Scheme 1), R_1 corresponds to the ohmic resistance of the electrolyte, R_2/Q_2 are related to the bulk SEI impedance, while R_3/Q_3 can be ascribed to the grain boundaries inside the SEI and between lithium and SEI layer. R_4/Q_4 are related to the charge transfer process at the lithium electrode/liquid electrolyte interface, across the SEI [28,29].



Scheme 1. Equivalent circuit.

In some cases, it was not possible to fit the low frequency portion. The equivalent circuit $R_1(R_2/Q_2)(R_3/Q_3)$ was used in these cases, and the contribution of the charge transfer was not included in the results. When it was not possible to fit the impedance plots as mentioned before, the simple $R_1(R_2/Q_2)$ equivalent circuit was used to describe the system. All the results are reported in Table A2. The gradual increase of the electrolyte resistance has been attributed by J. Woo et al. to the progressive electrolyte consumption during cycling [30]. This is more evident from time t_1 to time t_2 , which has a much longer time interval than that between t_0 and t_1 ; it also contains the cycles at higher current densities, during which more electrolyte decomposition is expected to occur. However, LP30- NH_4PF_6 behaves in the opposite way during the latter step. This anomaly could be due to the presence of a protic additive, which leads to a slight hydrogen evolution on the lithium interphase that increases the electrolyte resistance [31]. During the following cycles, the hydrogen gas is removed by reaction with lithium leading to a decrease in the electrolyte resistance. The impedance spectra before cycling (at t_0) further highlight differences among LP30- NH_4PF_6 and the other electrolytes (Figure 5a–d). An additional interphase is clearly evident in the spectra just after the assembly of LP30- NH_4PF_6 . At the same time, the cell with LP30- NH_4PF_6 possesses the lowest impedance. In general, the total cell impedance progressively decreases with cycling. This may be ascribed to the enlarged surface area of lithium electrodes due to the formation of dendritic morphology. LP30- NH_4PF_6 (Figure 5b) presents an inversion after t_1 , when the impedance increases. Nonetheless, the resistance values remain lower than those of other cells. An enhanced growth of a thick interlayer in consequence of the cycling at higher current density could explain this opposite trend. At t_1 , after 10 cycles, LP30- TEAPF_6 (Figure 5d) reaches an impedance value comparable to that of LP30 without additives (Figure 5a). It also shows a well-developed semicircle in the low frequency region, which is associated with the charge transfer. The only other value of charge transfer resistance obtained at t_1 is for LP30- NH_4PF_6 . The latter owns a resistance

one order of magnitude less than LP30-TEAPF₆. Apart from the nonideal capacitive features previously mentioned, the depressed and asymmetric shape of some semicircles could also be generated by slightly different contributions from the two electrodes. Although they should be equal, some small differences in the electrode surface could determine the presence of two almost identical, and therefore difficult to separate, semicircles. Based on the values of the exponent a , this interpretation is particularly true in the low frequency domain, where the charge transfer process occurs. This kind of asymmetry makes the fitting procedure more difficult, which is confirmed by the deposition/stripping cycles showing a correspondent lack of symmetry in the reduction and oxidation voltage profiles.

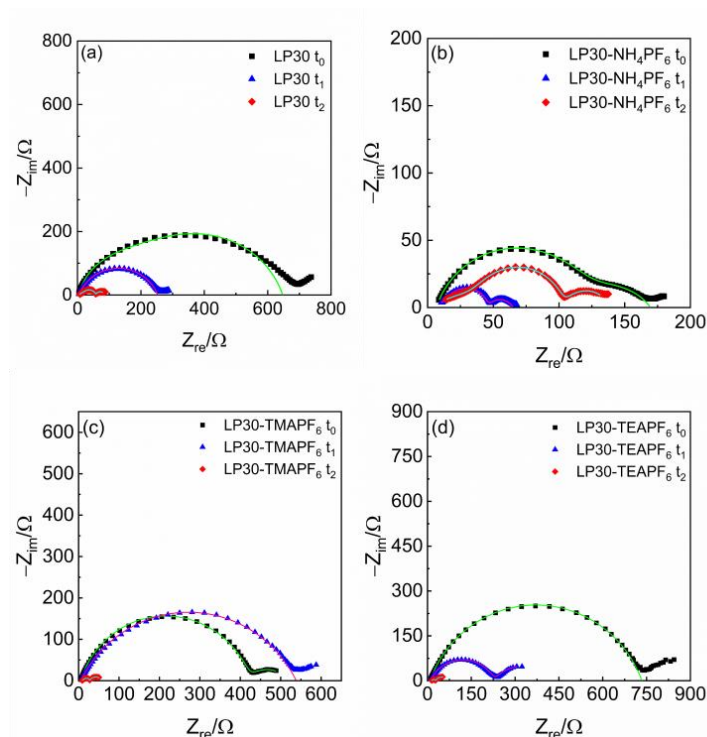


Figure 5. Electrochemical impedance spectra of Li || Li symmetric cells (a) LP30, (b) LP30-NH₄PF₆, (c) LP30-TMAPF₆, (d) LP30-TEAPF₆ after different cycling time. The green, red and cyan lines in the figures are the fitting results for the t_0 , t_1 and t_2 plots, respectively. The enlarged parts at high frequency of Figure 5a,c,d are in Figure A1.

From a comparison of impedance spectra at t_2 , with all plots fit with the same circuit, it is possible to note that the charge transfer resistance is not particularly affected by the presence of additives. LP30-TEAPF₆ still has the greatest resistance but shows no remarkable difference with respect to the others.

The impedance data are in good agreement with the polarization profiles obtained from the deposition/stripping cycles. The progression followed by the lithium anodes upon cycling is characterized by a significant increase in the surface area of the electrode. This could be coupled with partial loss of the mechanical integrity of the separator, which contributes to the decrease of the total impedance and polarization. Unlike the other electrolytes, the interphase of LP30-NH₄PF₆, which is already present at t_0 , continuously grows even after cycles at the high current density.

The equivalent circuits used to fit the impedance spectra of PC-based solutions are the same for the LP30-based solution set. The Nyquist plots are reported in Figure 6a–d, and the results of the fittings are in Table A3. The expected enhancement of the R_1 resistance of the electrolyte during cycling was not observed between t_0 and t_1 . After 10 cycles, all the cells present no changes or are less resistive. A relevant growth in R_1 occurs only at t_2 and becomes more evident for PC-TMAPF₆. This may occur because, in this case, the EIS

spectrum indicated as t_2 was taken after 945 cycles (ca. 950 h after assembly and cycling instead of 130 h).

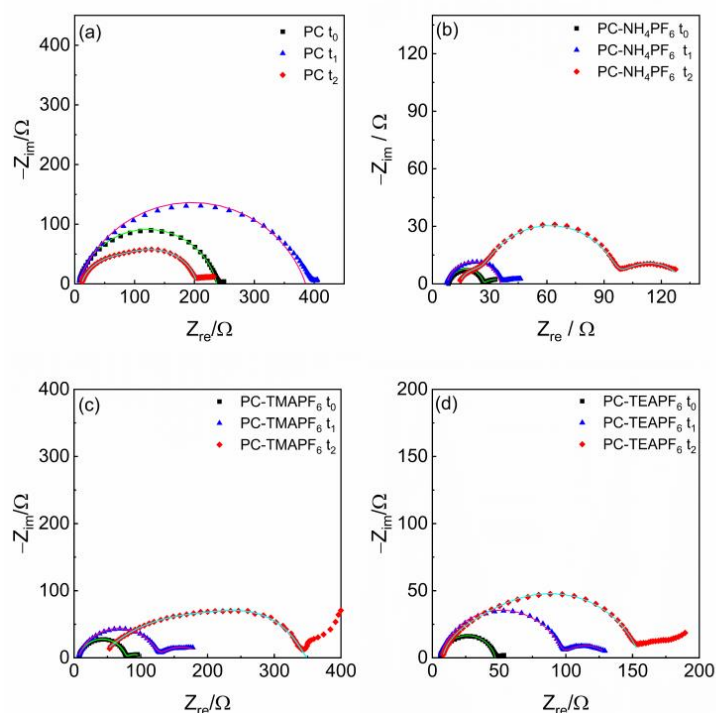


Figure 6. Electrochemical impedance spectra of Li|Li symmetric cells (a) PC, (b) PC-NH₄PF₆, (c) PC-TMAPF₆, (d) PC-TEAPF₆ after different cycling time. The green, red and cyan lines in the figures are the fitting results for the t_0 , t_1 and t_2 plots, respectively. The plot at t_2 in Figure 6c has been recorded at the end of the test reported in Figure 4c (after 945 total cycles).

The total impedance growth from t_0 to t_1 in all the cells is due to the development of a more resistive interphase. After the cycles at 0.500 mA cm^{-2} , the enhanced dendritic deposition is expected to generate the observed decrease in the impedance associated with the bulk surface interphase. However, we observed an increase in the overall resistance over cycling, with an evident growth of the grain boundary contribution in the solutions containing the additives. The resistance increase after high current density cycles suggests the formation of a thick, multigrain structured SEI.

3.3. Voltage Profile Analysis

The information obtained from EIS spectra supports the interpretation of the overvoltage profiles of subsequent lithium plating/stripping processes.

Typically, the deposition-stripping overpotential profile of a single electrode shows the first deposition process starting with a peak due to the high kinetic hindrance of the lithium nucleation on the smooth metal surface with a native passivation layer. In the following cycles, the intensity of this peak decreases due to the lower resistance of the already cycled lithium. After the nucleation peak, the overpotential decreases, evincing a more favourable lithium deposition than is possible when the incomplete passivation layer exposes fresh lithium and new lithium is preferentially deposited on it. On the other hand, the first stripping originates preferentially on the previously deposited lithium as it has a higher surface area and/or a not well-developed SEI. This partial lithium redissolution is the origin of the dendrite's erosion, which forms the electrically isolated lithium [32,33].

When all the freshly deposited lithium is completely dissolved or disconnected from the electrode as dead lithium, the stripping process takes place on old lithium, leading to an increase in overpotential. Specifically, the overpotential profile grows gradually as

lithium becomes more difficult to strip with the maximum overpotential associated with the bulk lithium electrode. In some cases, the overpotential decreases after the maximum overpotential due to the beginning of the pitting process, which induces preferential stripping from pitted areas, leading to more porous and roughened deposits [34].

All these phenomena produce the potential profile for a lithium electrode during deposition–stripping cycles. In a two-electrode cell, the working and counter electrode processes result in a voltage profile which is the sum of the contemporary contributions of the processes occurring at the two electrodes. The profile features previously described for the deposition and stripping processes at one electrode occur simultaneously at the two lithium electrodes and provide the resulting two-electrode cell overvoltage profile, as shown in Figure 7a, where in LP30 the simultaneous presence of the nucleation peak current on the counter electrode and the stripping from the smooth metal surface with a native passivation layer on the working electrode lead to a voltage profile characterized by a double peak shape, specifically at the highest current densities. During the deposition, the nucleation peak is evidenced because of the different dependency of the deposition overpotentials with current density, as modelled by Barton et al. in 1962 [35]. On the other hand, high stripping current density leads to a less uniform stripping, anticipating the stripping of the old lithium (second peak). Continuous cycling at the lowest current density forms a porous and low-density surface. After 600 cycles, the overpotential becomes constant because the deposition/stripping only occurs on the porous area of the electrodes. In the presence of tetraalkylammonium salts (Figure 7c,d), the voltage profiles at the lowest current appear quite flat from the first cycle. A smooth and flat lithium surface is attributed to uniform lithium deposition; supposedly, the freshly deposited lithium is the only one stripped. In that case, the overvoltage is constant because the stripping takes place on an area with constant surface resistance. This suggests a beneficial effect of the tetraalkylammonium additives on lithium cyclability.

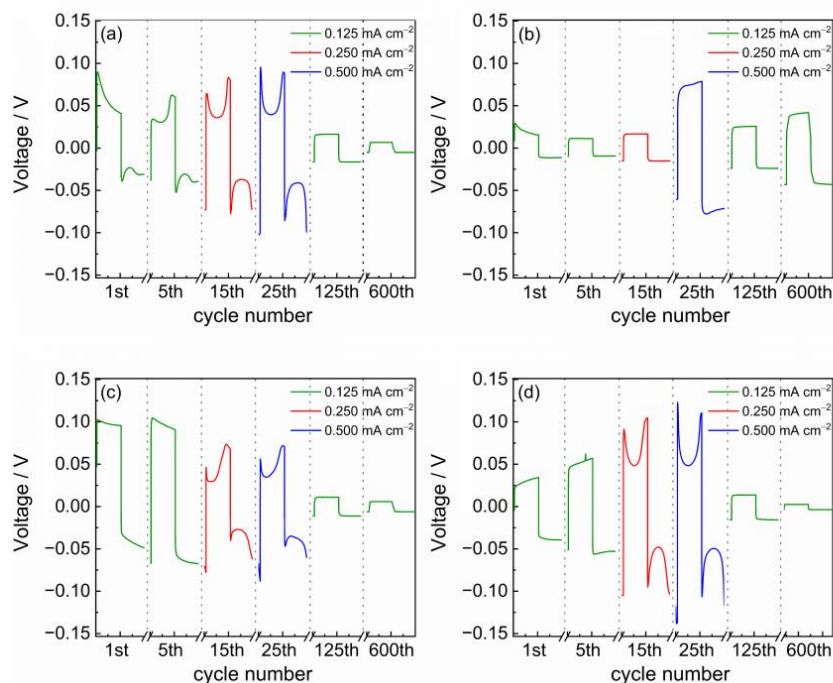


Figure 7. Selected overvoltage profiles of lithium deposition/stripping of Li | Li symmetric cells with (a) LP30, (b) LP30-NH₄PF₆, (c) LP30-TMAPF₆, (d) LP30-TEAPF₆ electrolytes at 0.125 mA cm⁻² (green), 0.250 mA cm⁻² (red) and 0.500 mA cm⁻² (blue).

Also, LP30-NH₄PF₆ shows a constant and flat profile (Figure 7b) at 0.125 and 0.25 mA cm⁻². At 0.500 mA cm⁻², a profile characterized by the features described for the LP30 measurement is visible. Coming back to 0.125 mA cm⁻², the overvoltage profile results are flat. The overvoltage slowly increases due to the gradually increasing of the surface resistance confirmed by EIS (Figure 5b at t₁ and t₂). This behaviour suggests a more limited formation of dendrites than in other LP30-based electrolytic systems.

The profile investigation was extended to PC-based electrolytes (Figure 8a–d). As shown in Figure 8a, the voltage profile in the PC is comparable to the LP30 electrolyte. However, it shows higher overvoltage, and at a high cycle number, the change in the shape of the voltage curve in the single cycle shows the gradual appearance of the typical arcing that can be associated with a hindered mass transport or a highly rough electrode surface (Figure 8a) [36,37]. This is also supported by the EIS, where PC shows the highest resistance and overvoltage attributed to the presence of dead lithium. In the presence of additives, the profiles do not show the arcing at a high cycle number (e.g., 600th cycle). Specifically, PC-TEAPF₆ shows the double peak shape that clearly arises from the lithium nucleation on one electrode and the lithium stripping onto the other, following the behaviour described for the first cycle of the LP30 electrolyte. This indicates that the lithium electrode was not eroded and did not show a porous deposit, even after 600 cycles. In addition, all the profiles (Figure 8b–d) show low hindrance to the lithium plating, indicated by the absence of the nucleation peak in the voltage profile. PC-NH₄PF₆ (Figure 8b) shows similar overvoltage to PC-TEAPF₆, with a slight arcing after prolonged cycling. By contrast, even if it shows the lowest overvoltage, PC-TMAPF₆ (Figure 8c) presented a slightly arched profile after continuous deposition-stripping, indicating a rougher lithium surface even after 600 cycles.

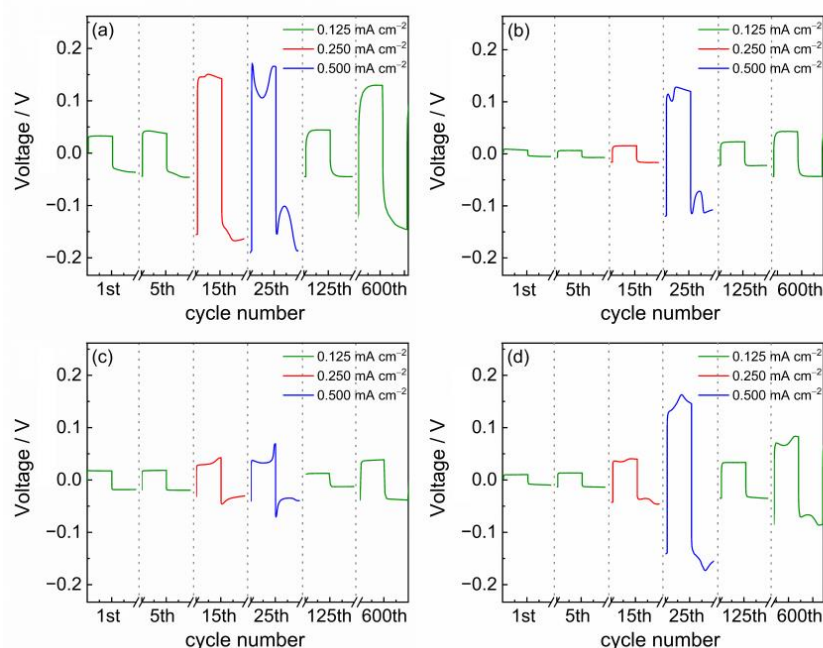


Figure 8. Selected overvoltage profiles of lithium deposition/stripping of Li | Li symmetric cells with (a) PC, (b) PC-NH₄PF₆, (c) PC-TMAPF₆, (d) PC-TEAPF₆ electrolytes at 0.125 mA cm⁻² (green), 0.250 mA cm⁻² (red) and 0.500 mA cm⁻² (blue).

3.4. Impedance Spectroscopy Investigation on Spontaneously Formed Interlayers

Two additional Li symmetric cells with PC and PC-NH₄PF₆ electrolytes were assembled and let rest for one week. During this time, EIS spectra were collected. The spectra are reported in Figure 9a,b. Considering a constant contribution related to the charge transfer resistance, the percentage growth of the interphase resistance has been reported in Figure 9c. The percentage has been calculated by considering the resistance values at-

tributed to the big semicircle. The initial value has been subtracted from the values at time t and divided by the initial value. The interphase changes more rapidly after 24 h in the presence of ammonium salt, which is reasonable considering its reactivity in the presence of lithium. Nonetheless, after a week, the impedance of the cell with the ammonium salt is still approximately one-third of the other (Figure 9c).

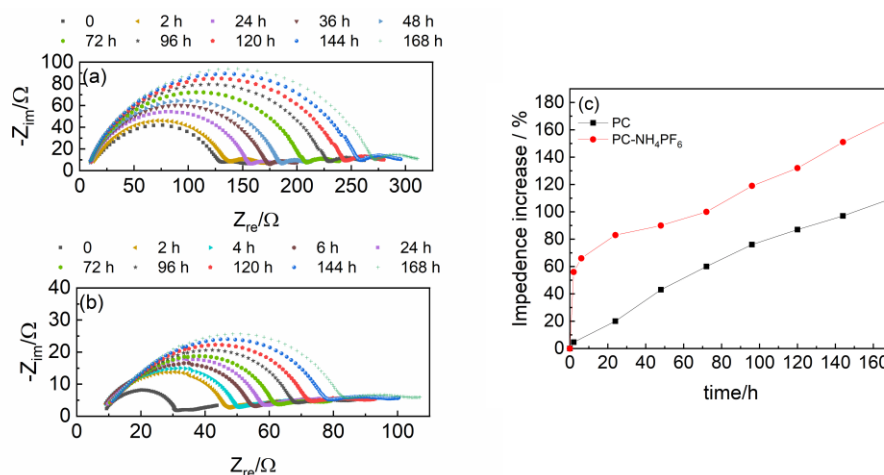


Figure 9. Nyquist plot of cells with (a) PC and (b) PC-NH₄PF₆ at different times in rest condition; (c) percentage of the interphase impedance increase over time with respect to the impedance at t_0 in PC (black) and in PC-NH₄PF₆ (red).

3.5. XRD Investigation

To better understand what occurred at the Li interphase, we immersed two lithium samples in LP30-NH₄PF₆ and PC-NH₄PF₆ solutions containing different concentrations, 50 mM and 250 mM, of ammonium salt. The samples became dark grey after a few minutes of immersion in the solutions (Figure A2). The only difference that is detectable to the human eye is a less intense but more prolonged gas evolution from the sample in PC, thus suggesting slower kinetics of the process. From the XRD analysis of the samples, which were sealed in glove box on glass slides with a mylar sheet, it is possible to notice an intense signal at about 26° due to mylar. The lithium disks immersed in LP30-NH₄PF₆ show a signal at 22° (Figure 10a,b) associated with the formation of Li₃N (reference pattern 00-002-0301_6). At the same time, the most intense signal of lithium at 36° (reference pattern 00-001-1131_3) decreases in intensity. This seems reasonable considering that the surface becomes passivated by a thick layer. Unfortunately, the mylar signal covers the region where other intense lithium nitride reflexes are expected. In PC, no signal related to the presence of Li₃N was collected. In this case, the signal of lithium decreased in intensity and almost disappeared in the sample immersed in the solution with 250 mM ammonium salt. This can be due to effects of both the sample orientation and lithium consumption. The reason we cannot see any Li₃N signal can be ascribed to slower kinetic hinderance of the layer formation. Even if it is thin, a nitride layer is expected to also be formed in PC-NH₄PF₆. The most relevant difference between the two carbonate systems is the salt, which may play some role in assisting the reaction. It should be noted that the XRD measurement has been performed with an unfavourable set up, with instrumentation designed to be used for powder samples. Thus, the detection of a relatively intense signal supporting the presence of Li₃N can be deemed a good result.

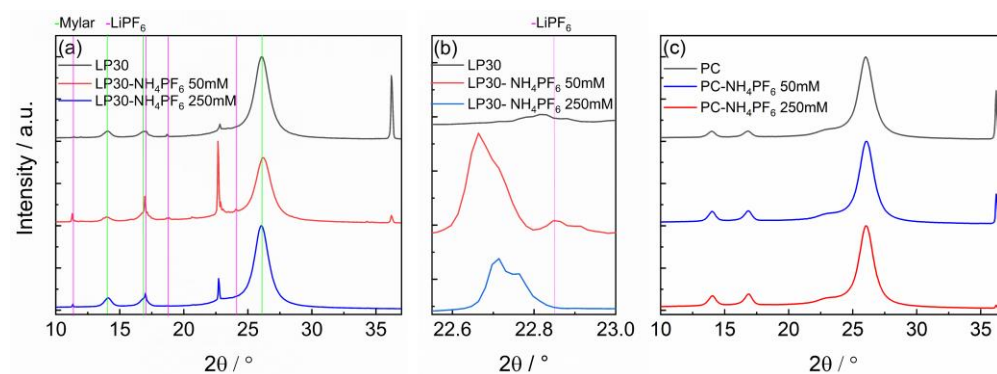


Figure 10. X-ray diffraction patterns of lithium samples after immersion in solution containing 50 and 250 mM NH_4PF_6 . (a) Sample immersed in LP30 with added NH_4PF_6 , (b) enlargement of signal at 22° ; (c) sample immersed in PC with added NH_4PF_6 .

3.6. SEM Images

SEM was used to investigate the morphology of cycled lithium electrodes. Additional cells in PC, PC- NH_4PF_6 , PC-TMAPF₆, and PC-TEAPF₆ were assembled. After 30 cycles at different current densities, the electrodes were disassembled in the glove box and mounted on the SEM holder. Figure 11a,b reports the SEM images of the lithium before contacting the electrolyte. It shows a flat surface with lines due to the sample lamination. After 30 cycles at different current densities in PC (Figure 11c,d), the lithium sample shows a grain-like morphology with grains diameter of ca. 1 μm . This indicates the inhomogeneous deposition achieved by using this electrolyte without additives. The metal electrode appears highly porous when cycled in PC- NH_4PF_6 (Figure 11e,f). The formation of pores (diameter ca. 10 μm) is ascribed to the reaction of lithium with the ammonium cation and the hydrogen produced at the interphase. The production of high porosity begins in the early stage of the galvanostatic cycles and increases the electrode surface area, thereby lowering the effective current density that is applied on the electrode. SEM images in tetraalkylammonium salts (Figure 11g–j) show a flat surface with less evident asperities, indicating the beneficial effect on the deposited lithium morphology. In particular, lithium cycled in PC-TMAPF₆ (Figure 11g,h) does not appear rough or grainy, even at high magnification. On the contrary, the sample appears rougher in PC-TEAPF₆ than in PC-TMAPF₆. This can be ascribed to the lower charge density of tetraethylammonium cation with respect to tetramethylammonium cation, which lowers the shielding ability of the TEAPF₆ additive.

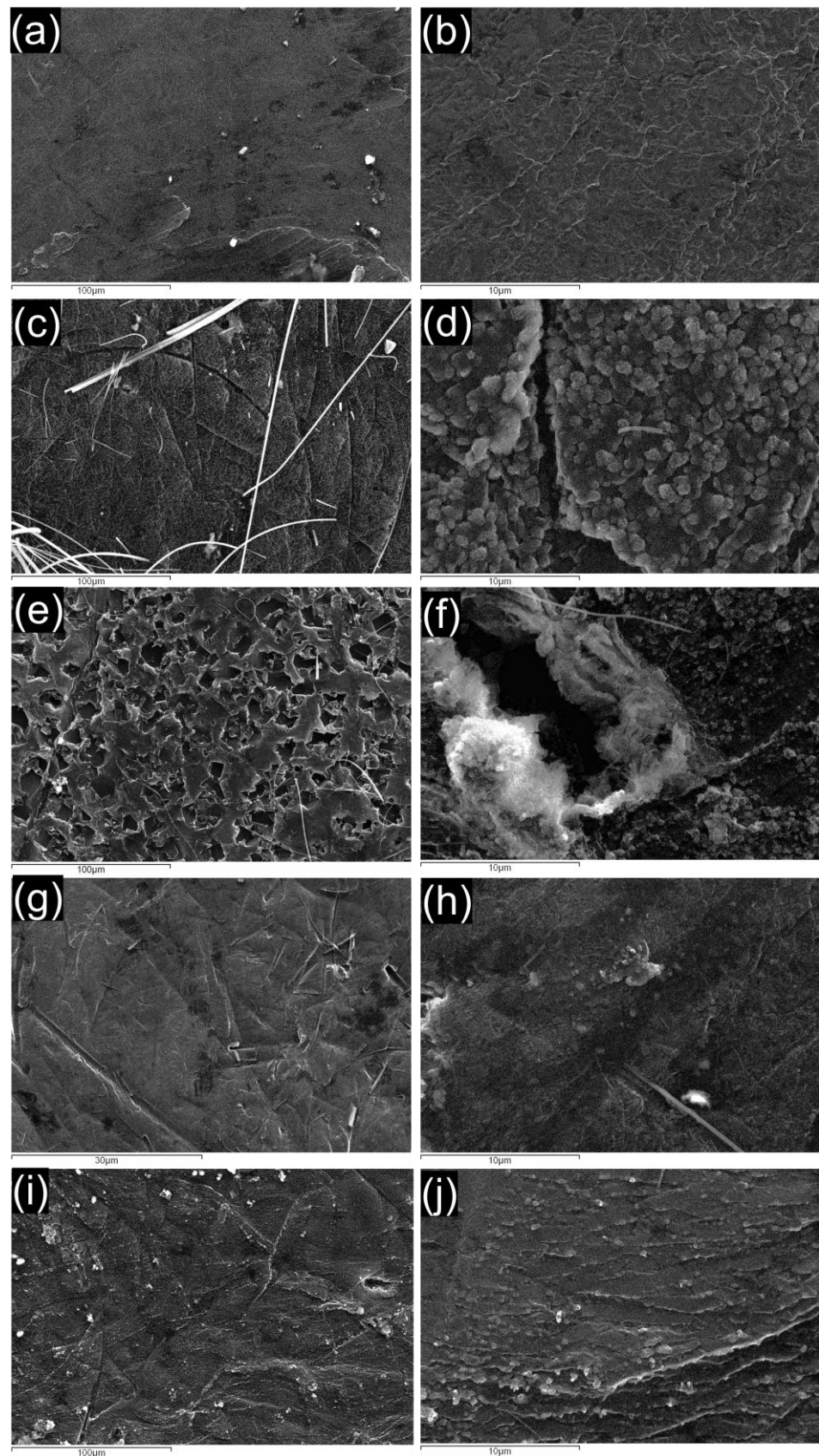


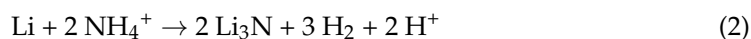
Figure 11. SEM images of pristine lithium (a,b) and cycled samples in (c,d) PC, (e,f) PC-NH₄PF₆, (g,h) PC-TMAPF₆, and (i,j) PC-TEAPF₆ at two magnification.

4. Discussion

In the long term, PC seems to suffer more than LP30 from the formation of dead lithium, with the hindrance of mass transport development as its consequence. The addition of NH_4PF_6 and TEAPF_6 is beneficial to the cell operation, resulting in a remarkable decrease of the total impedance, specifically of impedance associated with the SEI_{bulk} . The charge transfer resistance value, evaluated from the fitting of the plots at t_2 of PC- NH_4PF_6 and t_1 for PC- TEAPF_6 , agrees with the one obtained in LP30. The portion of the spectra of PC- NH_4PF_6 relative to the charge transfer is easier to fit. Although the semicircle is not easy to distinguish, it is not completely flat, unlike other cells. This indicates that the presence of the ammonium makes the two surfaces much more similar and even induces the deposition/stripping process.

PC-based electrolytes exhibit the tendency to develop higher polarization profiles because of prolonged cycling instead of showing diminishing impedance and overpotential, like LP30-based electrolytes do. This suggests that the deposition/stripping process could produce more electrically insulated lithium in the case of PC. However, it is necessary to also consider that, in the absence of LiPF_6 , as in the case of the PC solution, the integrity of the glass fibre separator is conserved for a longer time; this could result in a negligible contribution. All the additives presented seem to exert a positive effect, specifically in decreasing the tendency to develop high polarization and impedance. The combined chemical inertia shown in the background CVs, along with the beneficial effect of TMAPF_6 and TEAPF_6 , suggests an electrostatic shielding mechanism exerted by tetraalkylammonium salts. This can be particularly true in the PC- TEAPF_6 system, where the additive leads to a smooth deposit even after 600 cycles. In PC electrolytes, this attitude is suggested by a positive effect on the polarization profile, which is stabilized during deposition/stripping cycles. Meanwhile, it is less affected by the rise of the overvoltage related to the hindered mass transport caused by the formation of electrically insulated lithium. TMAPF_6 does not show any clear effect on the electrochemical behaviour of the cells. However, the voltage profiles in PC- TMAPF_6 show lower overvoltage, even at 0.500 mA cm^{-2} . LP30- TMAPF_6 behaves similarly to LP30, but the voltage profiles are less regular, with some abrupt changes. By virtue of the chemical similarity with TEAPF_6 , a possible beneficial action of TMAPF_6 cannot be excluded if used in higher concentration. Morphologic investigation in PC evidenced that tetraalkylammonium additive (especially TMAPF_6) leads to a more uniform lithium surface.

The action exerted by NH_4PF_6 is different and relies on direct reaction with lithium with a consequential variation in the chemical composition of the native SEI layer. One of the possible reactions occurring is based on the simple reaction of lithium with the ammonium cation to form Li_3N ,



although a more complex reaction mechanism that also involve the electrolyte cannot be excluded. The EIS measurements clearly indicate a less resistive behavior of the cell with NH_4PF_6 as well as the appearance of a well-developed interphase from the earliest stage of the measurements. The former effect could be due to the formation of a peculiar porous morphology of the electrode associated with the gas evolution during the chemical reaction, which could create preferential transport pathways across the passivation layer.

SEM images highlighted that NH_4PF_6 leads to a porous lithium morphology. The formation of micrometric pores is ascribed to the reaction of lithium with the ammonium cation and to the hydrogen produced at the interphase. The formation of highly porous lithium increases the surface area leading to a generally lower overvoltage (Figure 4b). In addition, the high surface area decreases the local current density applied to the lithium electrode. This can lead to a less dendritic lithium deposition justifying the stability of the cell over time. Considering that the formation of gas could be a potential safety issue, it will be interesting to investigate the possibility of performing a pretreatment of lithium anodes

beyond using the ammonium as an additive in solution. The addition of all the investigated additives does not seem to alter the charge transfer process at the level of the lithium electrode. The XRD observations confirmed the proposed mechanism for LP30-based electrolytes (2). On the contrary, the presence of nitride is not detected in PC, which could be due to the unfavourable analysis conditions. In fact, a passivation layer, whose chemical composition needs to be further investigated, is clearly formed in both cases. In addition, it needs to be clarified if the anion and/or the solvent have an active role during the reaction. Operando measurements are ongoing and will be the topic of future publications.

Finally, the preliminary measurements in Li||NMC cell with PC-based electrolyte with and without additives, reported in Figure A3 in Appendix A.1, evidence good capacity retention over cycling and coulombic efficiency, thus indicating no critical interactions of the tetraalkylammonium cations with the NMC cathode occur.

5. Conclusions

For the first time, ammonium and tetraalkylammonium salts have been investigated as additives for Li metal batteries with carbonate-based electrolytes. The investigated tetraalkylammonium salts, TMAPF₆ and TEAPF₆, are likely to exert an electrostatic shielding effect on the lithium deposition process, which is suggested in PC electrolyte by a positive effect on the polarization profile. On the other hand, NH₄PF₆ directly reacts with lithium with consequent variation in the chemical composition of the native SEI layer. The EIS measurements clearly indicate a less resistive behaviour of the cell with NH₄PF₆ and the appearance of a well-developed interphase from the earliest stage of the measurements. However, a more complex reaction mechanism also involving an active role of the electrolyte cannot be excluded. Preliminary tests in an Li||NMC cell with PC-based electrolytes demonstrated that the cathode is stable in contact with tetraalkylammonium cations as evinced by the high coulombic efficiency and charge retention over galvanostatic charge and discharge cycles. On the contrary, in the presence of NH₄PF₆, the cell shows a low coulombic efficiency over prolonged cycles, thus indicating that the higher salt reactivity may affect the overall cycling stability of the cell. Operando investigations are necessary to highlight better the reactions occurring at the Li interphase and will be the object of further studies.

Author Contributions: Conceptualization, C.A.; methodology, D.D.C., L.B., and G.L.; validation, D.D.C., L.B., and G.L.; formal analysis, D.D.C., L.B., and G.L.; investigation, D.D.C., L.B., and G.L.; data curation, D.D.C., L.B., and G.L.; writing—original draft preparation, C.A.; writing—review and editing, D.D.C., L.B., and G.L.; supervision, C.A.; project administration, C.A.; funding acquisition, C.A. All authors have read and agreed to the published version of the manuscript.

Funding: This research was funded by MiSE-ENEA PTR 2019–2021—Research of Electrical System (RSE) “Development of stable electrodes for Na ion batteries and characterization of the Li anode interphase” as activity of WP1-LA77 “Characterization of the Li/electrolyte interphase in full cell” and G.L. acknowledges the Department of Excellence program financed by the Ministry of Education, University and Research (MIUR, L. 232 del 01/12/2016) for the doctoral scholarship.

Data Availability Statement: Not applicable.

Conflicts of Interest: The authors declare no conflict of interest.

Appendix A

Table A1. Reduction and oxidation voltage data obtained from cyclic voltammetry of lithium plating/stripping.

Electrolyte	Reduction _{onset} /mV		Oxidation _{peak} /mV	
	1st Cycle	10th Cycle	1st Cycle	10th Cycle
LP30	−100	−100	150	160
LP30-NH ₄ PF ₆	−75	−80	160	150
LP30-TMAPF ₆	−100	−90	120	190
LP30-TEAPF ₆	−100	−90	120	190
PC	−140	−100	115	130
PC-NH ₄ PF ₆	−90	−100	80	115
PC-TMAPF ₆	−115	−115	130	110
PC-TEAPF ₆	−135	−125	115	115

Table A2. Fitting parameters of the impedance spectra over deposition/stripping tests of Li || Li cells with LP30-based solutions. t_0 = before test, t_1 = after 10 cycles at 0.125 mA cm^{−2}, t_2 = after additional 10 cycles at 0.250 mA cm^{−2}, 100 cycles at 0.500 mA cm^{−2} and 10 cycles at 0.125 mA cm^{−2}. The fitting data with the highest relative errors are reported in grey.

LP30	R ₁ /Ω	R ₂ /Ω	Q ₂ /F s ^{a−1} a	R ₃ /Ω	Q ₃ /F s ^{a−1} a	R ₄ /Ω	Q ₄ /F s ^{a−1} a
t ₀	3.4 ± 0.3	160 ± 90	(2.1 ± 0.7)·10 ^{−6} 0.88 ± 0.07	500 ± 100	(1.0 ± 0.2)·10 ^{−5} 0.79 ± 0.08		
t ₁	4.1 ± 0.2	249 ± 3	(7.7 ± 0.4)·10 ^{−6} 0.759 ± 0.005				
t ₂	6.6 ± 0.2	11 ± 1	(9 ± 3) 10 ^{−6} 0.80 ± 0.03	40 ± 1	(2.4 ± 0.2) 10 ^{−5} 0.02	29 ± 3	(1.0 ± 0.1)·10 ^{−2} 0.77 ± 0.05
LP30-NH ₄ PF ₆	R ₁ /Ω	R ₂ /Ω	Q ₂ /F s ^{a−1} a	R ₃ /Ω	Q ₃ /F s ^{a−1} a	R ₄ /Ω	Q ₄ /F s ^{a−1} a
t ₀	6.63 ± 0.09	112 ± 3	(3.3 ± 0.2) 10 ^{−6} 0.808 ± 0.006	51 ± 5	(7 ± 1) 10 ^{−4} 0.60 ± 0.05		
t ₁	6 ± 1	9 ± 3	(4 ± 6) 10 ^{−5} 0.6 ± 0.1	31 ± 2	(3.8 ± 0.3)·10 ^{−6} 0.90 ± 0.02	19.4 ± 0.4	(3.8 ± 0.2) 10 ^{−3} 0.69 ± 0.01
t ₂	3.9 ± 0.9	47 ± 6	(2.0 ± 0.7) 10 ^{−4} 0.43 ± 0.03	55 ± 4	(1.5 ± 0.1) 10 ^{−5} 0.93 ± 0.02	33 ± 2	(7.3 ± 0.5) 10 ^{−3} 0.78 ± 0.04
LP30-TMAPF	R ₁ /Ω	R ₂ /Ω	Q ₂ /F s ^{a−1} a	R ₃ /Ω	Q ₃ /F s ^{a−1} a	R ₄ /Ω	Q ₄ /F s ^{a−1} a
t ₀	5.3 ± 0.2	418 ± 8	(4.5 ± 0.3)·10 ^{−6} 0.816 ± 0.006	90 ± 50	(8 ± 3) 10 ^{−3} 0.60 ± 0.05		
t ₁	5.4 ± 0.3	533 ± 7	(1.21 ± 0.06)·10 ^{−5} 0.708 ± 0.06	31 ± 2	(3.8 ± 0.3) 10 ^{−6} 0.90 ± 0.02	19.4 ± 0.4	(3.8 ± 0.2) 10 ^{−3} 0.69 ± 0.01
t ₂	9.6 ± 0.1	4 ± 1	(2 ± 2) 10 ^{−6} 1.0 ± 0.09	14 ± 1	(2.1 ± 0.5) 10 ^{−5} 0.88 ± 0.04	30 ± 2	(1.9 ± 0.1) 10 ^{−3} 0.69 ± 0.03
LP30-TEAPF ₆	R ₁ /Ω	R ₂ /Ω	Q ₂ /F s ^{a−1} a	R ₃ /Ω	Q ₃ /F s ^{a−1} a	R ₄ /Ω	Q ₄ /F s ^{a−1} a
t ₀	8.6 ± 0.2	725 ± 6	(3.4 ± 0.1)·10 ^{−6} 0.78 ± 0.04				
t ₁	9.6 ± 0.2	219 ± 2	(9.3 ± 0.5)·10 ^{−6} 0.722 ± 0.005	180 ± 50	(9.4 ± 0.9)·10 ^{−6} 0.61 ± 0.07		
t ₂	14.7 ± 0.1	4 ± 1	(2 ± 2) 10 ^{−6} 1.0 ± 0.09	8 ± 1	(2.4 ± 0.6)·10 ^{−5} 0.89 ± 0.04	47 ± 2	(2.47 ± 0.06)·10 ^{−2} 0.62 ± 0.01

Table A3. Fitting parameters of the impedance spectra over deposition/stripping tests of Li | Li cells with PC-based solutions. t_0 = before test, t_1 = after 10 cycles at 0.125 mA cm^{-2} , t_2 = after additional 10 cycles at 0.250 mA cm^{-2} , 100 cycles at 0.500 mA cm^{-2} and 10 cycles at 0.125 mA cm^{-2} . The fitting data with the highest relative errors are reported in grey.

PC	R_1/Ω	R_2/Ω	$Q_2/F \text{ s}^{a-1}$ a	R_3/Ω	$Q_3/F \text{ s}^{a-1}$ a	R_4/Ω	$Q_4/F \text{ s}^{a-1}$ a
t_0	6.4 ± 0.2	231 ± 2	$(1.65 \pm 0.09) 10^{-6}$ 0.853 ± 0.005				
t_1	5.7 ± 0.3	380 ± 4	$(3.4 \pm 0.2) 10^{-6}$ 0.793 ± 0.006				
t_2	11.56 ± 0.09	74 ± 6	$(4.1 \pm 0.3) 10^{-6}$ 0.832 ± 0.009	119 ± 7	$(1.5 \pm 0.1) 10^{-5}$ 0.85 ± 0.02		
PC-NH ₄ PF ₆	R_1/Ω	R_2/Ω	$Q_2/F \text{ s}^{a-1}$ a	R_3/Ω	$Q_3/F \text{ s}^{a-1}$ a	R_4/Ω	$Q_4/F \text{ s}^{a-1}$ a
t_0	8.6 ± 0.2	17.1 ± 0.7	$(4 \pm 1) 10^{-6}$ 0.90 ± 0.02	16 ± 10	$(9 \pm 3) 10^{-2}$ 0.3 ± 0.1		
t_1	7.5 ± 0.2	28 ± 1	$(4.5 \pm 0.9) 10^{-6}$ 0.88 ± 0.02	15 ± 5	$(1.5 \pm 0.1) 10^{-5}$ 0.85 ± 0.02		
t_2	14.2 ± 0.2	12.3 ± 0.7	$(5 \pm 2) 10^{-6}$ 0.85 ± 0.03	70 ± 1	$(1.6 \pm 0.1) 10^{-5}$ 0.89 ± 0.01	36 ± 3	$(9.7 \pm 0.8) \cdot 10^{-3}$ 0.67 ± 0.05
PC-TMAPF ₆	R_1/Ω	R_2/Ω	$Q_2/F \text{ s}^{a-1}$ a	R_3/Ω	$Q_3/F \text{ s}^{a-1}$ a	R_4/Ω	$Q_4/F \text{ s}^{a-1}$ a
t_0	6.5 ± 0.1	70 ± 1	$(2.3 \pm 0.2) 10^{-6}$ 0.85 ± 0.01	28 ± 6	$(2.4 \pm 0.4) 10^{-2}$ 0.43 ± 0.08		
t_1	5.9 ± 0.1	120 ± 2	$(4.5 \pm 0.3) 10^{-6}$ 0.52 ± 0.01	71 ± 8	$(8.1 \pm 0.9) 10^{-3}$ 1.0 ± 0.1		
t_2 *	38.5 ± 0.5	238 ± 13	$(2.7 \pm 0.2) 10^{-5}$ 0.56 ± 0.01	74 ± 12	$(2.5 \pm 0.3) 10^{-5}$ 0.92 ± 0.04		
PC-TEAPF ₆	R_1/Ω	R_2/Ω	$Q_2/F \text{ s}^{a-1}$ a	R_3/Ω	$Q_3/F \text{ s}^{a-1}$ a	R_4/Ω	$Q_4/F \text{ s}^{a-1}$ a
t_0	5.6 ± 0.2	41.6 ± 0.6	$(3.7 \pm 0.5) 10^{-6}$ 0.86 ± 0.01				
t_1	5.4 ± 0.1	91 ± 1	$(4.1 \pm 0.3) 10^{-6}$ 0.835 ± 0.007	35 ± 5	$(1.0 \pm 0.2) 10^{-2}$ 0.58 ± 0.08		
t_2	7.5 ± 0.1	23 ± 8	$(5 \pm 2) 10^{-6}$ 0.89 ± 0.05	130 ± 10	$(1.5 \pm 0.2) 10^{-6}$ 0.80 ± 0.03		

* after additional 815 cycles at 0.125 mA cm^{-2} .

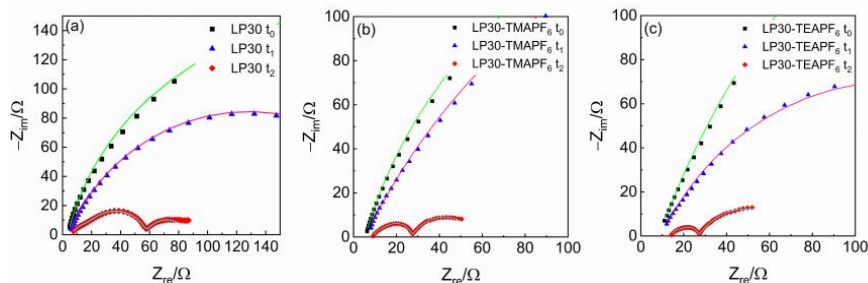


Figure A1. Enlarged view at high frequency of the Nyquist plot of Figure 5a,c,d. The green, red and cyan lines in the figures are the fitting results for the t_0 , t_1 and t_2 plots, respectively.

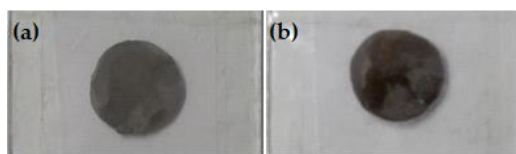


Figure A2. Lithium disk samples immersed for 2 days in (a) LP30 and (b) PC, both with the addition of 250 mM NH_4PF_6 .

Appendix A.1. Test in Li || NMC Cells

Preliminary galvanostatic charge/discharge cycles of cells with lithium metal anode and NMC cathode have been performed. The cathodes are made of NMC, PVdF, and C65 carbon in the ratio of 8:1:1. Coin cells (1.13 cm^2) were assembled with electrodes having mass loading ca. $8.2 \text{ mg}_{\text{NMC}} \text{ cm}^{-2}$. The tests were carried out at room temperature (near $22 \text{ }^\circ\text{C}$) by constant current–constant voltage charge and constant current discharge between 3.0 and 4.2 V. Three cycles at C/10 C-rate were performed, followed by cycles at C/2 C-rate. The capacity retention and the coulombic efficiency of the cells with PC electrolyte and with PC- NH_4PF_6 , PC-TMAPF₆, and PC-TEAPF₆, are shown in Figure A2. The cells show minor differences concerning the capacity retention, and those with alkylammonium additives are the best performing. Other than PC- NH_4PF_6 , all cells showed coulombic efficiency values close to 99%, which indicates no critical interactions between tetraalkylammonium ions and NMC cathode. The cell with the NH_4PF_6 additive behaves like the cell without additives in terms of capacity retention, but with a worse coulombic efficiency, especially over prolonged cycling. It is likely that the chemical reaction of NH_4PF_6 at the Li interface forms by-products that negatively affect cell stability. This suggests the possibility of using this salt in lower concentrations, or eventually in the same concentration during the initial cycles only, to form a good SEI, and then replacement the electrolyte with a pure PC-LiTFSI solution.

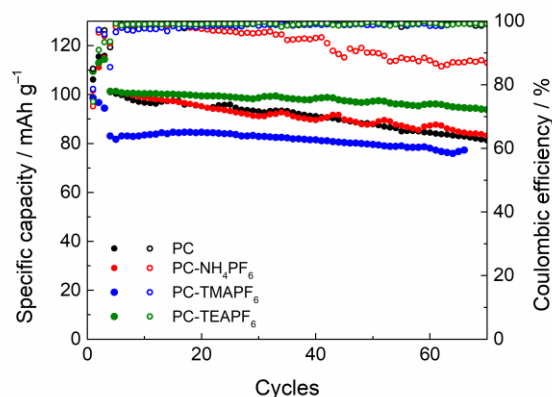


Figure A3. Capacity retention (full circles) and coulombic efficiency (open circles) data of Li || NMC cells with PC and PC- NH_4PF_6 electrolytes over testing at C/2, after two formation cycles at C/10 C-rate.

References

- Zhang, H.; Li, C.; Eshetu, G.G.; Laruelle, S.; Grugeon, S.; Zanghi, K.; Julien, C.; Mauger, A.; Guyomard, D.; Rojo, T.; et al. From Solid-Solution Electrodes and the Rocking-Chair Concept to Today's Batteries. *Angew. Chem.* **2020**, *132*, 542–546. [CrossRef]
- Xie, J.; Lu, Y.-C. A Retrospective on Lithium-ion Batteries. *Nat. Commun.* **2020**, *11*, 2499. [CrossRef] [PubMed]
- Steen, M.; Di Persio, F.; Boon-Brett, L.; Lebedeva, N.; EU Competitiveness in Advanced Li-Ion Batteries for E-Mobility and Stationary Storage Applications: Opportunities and Actions. Publications Office. 2018. Available online: <https://data.europa.eu/doi/10.2760/75757> (accessed on 1 December 2022).
- Aurbach, D.; Ein-Ely, Y.; Zaban, A. The Surface Chemistry of Lithium Electrodes in Alkyl Carbonate Solutions. *J. Electrochem. Soc.* **1994**, *141*, L1–L3. [CrossRef]

5. Aurbach, D. Review of Selected Electrode–Solution Interactions Which Determine the Performance of Li and Li Ion Batteries. *J. Power Sources* **2000**, *89*, 206–218. [[CrossRef](#)]
6. Peled, E.; Menkin, S. SEI: Past, Present and Future. *J. Electrochem. Soc.* **2017**, *164*, A1703–A1719. [[CrossRef](#)]
7. Ein-Eli, Y. A New Perspective on the Formation and Structure of the Solid Electrolyte Interface at the Graphite Anode of Li-Ion Cells. *Electrochem. Solid-State Lett.* **1999**, *2*, 212. [[CrossRef](#)]
8. Selvamani, V.; Suryanarayanan, V.; Velayutham, D.; Gopukumar, S. Asymmetric tetraalkyl ammonium cation-based ionic liquid as an electrolyte for lithium-ion battery applications. *J. Solid State Electrochem.* **2016**, *20*, 2283–2293. [[CrossRef](#)]
9. Li, J.; Liu, S.; Cui, Y.; Zhang, S.; Wu, X.; Xiang, J.; Li, M.; Wang, X.; Xia, X.; Gu, C.; et al. Potassium Hexafluorophosphate Additive Enables Stable Lithium–Sulfur Batteries. *ACS Appl. Mater. Interfaces* **2020**, *12*, 56017–56026. [[CrossRef](#)]
10. Chazalviel, J.-N. Electrochemical Aspects of the Generation of Ramified Metallic Electrodeposits. *Phys. Rev. A* **1990**, *42*, 7355–7367. [[CrossRef](#)]
11. Peled, E. The Electrochemical Behavior of Alkali and Alkaline Earth Metals in Nonaqueous Battery Systems—The Solid Electrolyte Interphase Model. *J. Electrochem. Soc.* **1979**, *126*, 2047–2051. [[CrossRef](#)]
12. Jana, A.; Woo, S.I.; Vikrant, K.S.N.; García, R.E. Electrochemomechanics of Lithium Dendrite Growth. *Energy Environ. Sci.* **2019**, *12*, 3595–3607. [[CrossRef](#)]
13. Ren, W.; Zheng, Y.; Cui, Z.; Tao, Y.; Li, B.; Wang, W. Recent Progress of Functional Separators in Dendrite Inhibition for Lithium Metal Batteries. *Energy Stor. Mater.* **2021**, *35*, 157–168. [[CrossRef](#)]
14. Chen, S.; Li, Y.; Wang, Y.; Li, Z.; Peng, C.; Feng, Y.; Feng, W. Cross-linked Single-Ion Solid Polymer Electrolytes with Alternately Distributed Lithium Sources and Ion-Conducting Segments for Lithium Metal Batteries. *Macromolecules* **2021**, *54*, 9135–9144. [[CrossRef](#)]
15. Zhang, X.; Wang, A.; Liu, X.; Luo, J. Dendrites in Lithium Metal Anodes: Suppression, Regulation, and Elimination. *Acc. Chem. Res.* **2019**, *52*, 3223–3232. [[CrossRef](#)]
16. Ota, H.; Shima, K.; Ue, M.; Yamaki, J. Effect of vinylene carbonate as additive to electrolyte for lithium metal anode. *Electrochim. Acta* **2004**, *49*, 565–572. [[CrossRef](#)]
17. Heine, J.; Hilbig, P.; Qi, X.; Niehoff, P.; Winter, M.; Bieker, P. Fluoroethylene Carbonate as Electrolyte Additive in Tetraethylene Glycol Dimethyl Ether Based Electrolytes for Application in Lithium Ion and Lithium Metal Batteries. *J. Electrochem. Soc.* **2015**, *162*, A1094–A1101. [[CrossRef](#)]
18. Mogi, R.; Inaba, M.; Jeong, S.; Iriyama, Y.; Abe, T.; Ogumi, Z. Effects of some organic additives on lithium deposition in propylene carbonate. *J. Electrochem. Soc.* **2002**, *149*, A1578–A1583. [[CrossRef](#)]
19. Zhang, X.-Q.; Cheng, X.-B.; Chen, X.; Yan, C.; Zhang, Q. Fluoroethylene Carbonate Additives to Render Uniform Li Deposits in Lithium Metal Batteries. *Adv. Funct. Mater.* **2017**, *27*, 1605989. [[CrossRef](#)]
20. Zhang, H.; Eshetu, G.G.; Judez, X.; Li, C.; Rodriguez-Martínez, L.M.; Armand, M. Electrolyte Additives for Lithium Metal Anodes and Rechargeable Lithium Metal Batteries: Progress and Perspectives. *Angew. Chem. Int. Ed.* **2018**, *57*, 15002–15027. [[CrossRef](#)]
21. Wang, A.; Kadam, S.; Li, H.; Shi, S.; Qi, Y. Review on modeling of the anode solid electrolyte interphase (SEI) for lithium-ion batteries. *Npj Comput. Mater.* **2018**, *4*, 15. [[CrossRef](#)]
22. Wang, Z.; Wang, Y.; Wu, C.; Pang, W.K.; Mao, J.; Guo, Z. Constructing nitrated interfaces for stabilizing Li metal electrodes in liquid electrolytes. *Chem. Sci.* **2021**, *12*, 8945–8966. [[CrossRef](#)]
23. Baloch, M.; Shanmukaraj, D.; Bondarchuk, O.; Bekaert, E.; Rojo, T.; Armand, M. Variations on Li₃N Protective Coating Using Ex-Situ and In-Situ Techniques for Li Degrees in Sulphur Batteries. *Energy Stor. Mater.* **2017**, *9*, 141–149.
24. Tiyyapiboonchaiya, C.; Pringle, J.M.; Sun, J.; Byrne, N.; Howlett, P.C.; MacFarlane, D.R.; Forsyth, M. The zwitterion effect in high-conductivity polyelectrolyte materials. *Nat. Mater.* **2004**, *3*, 29–32. [[CrossRef](#)] [[PubMed](#)]
25. Li, S.; Zhang, W.; Wu, Q.; Fan, L.; Wang, X.; Wang, X.; Shen, Z.; He, Y.; Lu, Y. Synergistic Dual-Additive Electrolyte Enables Practical Lithium–Metal Batteries. *Angew. Chem. Int. Ed.* **2020**, *59*, 14935–14941. [[CrossRef](#)] [[PubMed](#)]
26. Ding, F.; Xu, W.; Graff, G.L.; Zhang, J.; Sushko, M.L.; Chen, X.; Shao, Y.; Engelhard, M.H.; Nie, Z.; Xiao, J.; et al. Dendrite-Free Lithium Deposition via Self-Healing Electrostatic Shield Mechanism. *J. Am. Chem. Soc.* **2013**, *135*, 4450–4456. [[CrossRef](#)]
27. Lin, D.; Liu, Y.; Pei, A.; Cui, Y. Nanoscale Perspective: Materials Designs and Understandings in Lithium Metal Anodes. *Nano Res.* **2017**, *10*, 4003–4026. [[CrossRef](#)]
28. Busche, M.R.; Drossel, T.; Leichtweiss, T.; Weber, D.A.; Falk, M.; Schneider, M.; Reich, M.-L.; Sommer, H.; Adelhelm, P.; Janek, J. Dynamic Formation of a Solid-Liquid Electrolyte Interphase and Its Consequences for Hybrid-Battery Concepts. *Nat. Chem.* **2016**, *8*, 426–434. [[CrossRef](#)] [[PubMed](#)]
29. Hu, Z.; Zhang, S.; Dong, S.; Li, Q.; Cui, G.; Chen, L. Self-Stabilized Solid Electrolyte Interface on a Host-Free Li-Metal Anode toward High Areal Capacity and Rate Utilization. *Chem. Mater.* **2018**, *30*, 4039–4047. [[CrossRef](#)]
30. Woo, J.-J.; Maroni, V.A.; Liu, G.; Vaughey, J.T.; Gosztola, D.J.; Amine, K.; Zhang, Z. Symmetrical Impedance Study on Inactivation Induced Degradation of Lithium Electrodes for Batteries Beyond Lithium-Ion. *J. Electrochem. Soc.* **2014**, *161*, A827–A830. [[CrossRef](#)]
31. Metzger, M.; Strehle, B.; Solchenbach, S.; Gasteiger, H.A. Origin of H₂ Evolution in LIBs: H₂O Reduction vs. Electrolyte Oxidation. *J. Electrochem. Soc.* **2016**, *163*, A798–A809. [[CrossRef](#)]
32. Naoi, K.; Mori, M.; Shinagawa, Y. Study of Deposition and Dissolution Processes of Lithium in Carbonate-Based Solutions by Means of the Quartz-Crystal Microbalance. *J. Electrochem. Soc.* **1996**, *143*, 2517–2522. [[CrossRef](#)]

33. Xu, K. Nonaqueous Liquid Electrolytes for Lithium-Based Rechargeable Batteries. *Chem. Rev.* **2004**, *104*, 4303–4418. [[CrossRef](#)]
34. Bieker, G.; Winter, M.; Bieker, P. Electrochemical in situ investigations of SEI and dendrite formation on the lithium metal anode. *Phys. Chem. Chem. Phys.* **2015**, *17*, 8670–8679. [[CrossRef](#)]
35. Barton, J.L.; Bockris, J.O. The electrolytic growth of dendrites from ionic solutions. *Proc. R. Soc. London Ser. A* **1962**, *268*, 485–505.
36. Chen, K.-H.; Wood, K.N.; Kazyak, E.; LePage, W.S.; Davis, A.L.; Sanchez, A.J.; Dasgupta, N.P. Dead Lithium: Mass Transport Effects on Voltage, Capacity, and Failure of Lithium Metal Anodes. *J. Mater. Chem. A* **2017**, *5*, 11671–11681. [[CrossRef](#)]
37. Li, Z.; Ji, W.; Wang, T.-X.; Ding, X.; Han, B.-H.; Feng, W. Maximized lithiophilic carbonyl units in covalent organic frameworks as effective Li ion regulators for lithium metal batteries. *Chem. Eng. J.* **2022**, *437*, 135293. [[CrossRef](#)]

Disclaimer/Publisher’s Note: The statements, opinions and data contained in all publications are solely those of the individual author(s) and contributor(s) and not of MDPI and/or the editor(s). MDPI and/or the editor(s) disclaim responsibility for any injury to people or property resulting from any ideas, methods, instructions or products referred to in the content.